

미세다공성 Zn(II)-MOF의 아세틸렌 선택 흡착과 LL-37을 이용한 간암에 대한 항암효과 연구

Xiu-Qin Wei, Shuan-Yuan Yang^{*,†}, Xiao-Xia Li^{**}, and Mei-Li Xu^{**}

Department of Infections, Wuwei People's Hospital

*Department of Hepatobiliary Surgery, Tongchuan People's Hospital

**Department of Medicine, Hebei Hospital

(2021년 6월 19일 접수, 2021년 8월 2일 수정, 2021년 8월 18일 채택)

Microporous Zn(II)-MOF for Selective C₂H₂ Adsorption and Anti-cancer Activity on Liver Cancer Combined with LL-37

Xiu-Qin Wei, Shuan-Yuan Yang^{*,†}, Xiao-Xia Li^{**}, and Mei-Li Xu^{**}

Department of Infections, Wuwei People's Hospital, Wuwei, Gansu 727031, China

*Department of Hepatobiliary Surgery, Tongchuan People's Hospital, Tongchuan, Shaanxi 733000, China

**Department of Medicine, Hebei Hospital, Shijiazhuang, Hebei 050000, China

(Received June 19, 2021; Revised August 2, 2021; Accepted August 18, 2021)

Abstract: By employment of a semi-rigid carboxylic acid ligand 5,5'-(5-carboxy-1,3-phenylene)bis(azanediy)diisophthalic acid (H₃L) with the -NH- joints, a new porous metal-organic framework (MOF) based on Zn(II) ions as nodes has been generated in success, and its chemical formula is {[Zn₃(μ₃-OH)(L)(H₂O)₃]·3DEF·H₂O}_n (**1**). Owing to its Lewis basic -NH- joints and the π-electron-rich benzene rings on the skeleton, the activated complex **1** offers a favourable pore environment for binding C₂H₂ in preference to CO₂ and CH₄. The inhibitory activity of compound on the liver cancer viability was determined through exploiting the Cell Counting Kit-8 kit. Afterwards, the invasion and migration ability for the liver cancer cells was measured after indicated treatment. Multiple binding interactions are identified by performing the molecular docking simulation, indicating the stabilization effect of the Zn complex towards the target protein, and therefore, the proposed drug molecule exhibits good anticancer activities.

Keywords: metal-organic framework, porous framework, gas separation, liver cancer, molecular docking.

Introduction

Primary carcinoma of liver (hereinafter referred to as liver cancer) is one of the common malignant tumors in our country.¹ According to statistics recently, the annual mortality rate of liver cancer in China was 20.37 per 100000, ranking second in the ranking of malignant tumor deaths, second only to lung cancer in cities, and second only to gastric cancer in rural areas.² The maturity of surgical techniques and the development of non-surgical treatment methods such as various local treatments have significantly improved the prognosis of liver cancer compared with the past.³ However, new candidates for

the liver cancer therapy were still need to be explored. LL-37 is the only Cathelicidin antimicrobial peptide found in the human body. It has a cancer-promoting effect in ovarian cancer, malignant melanoma, skin squamous cell carcinoma, prostate cancer and other tumors, but as a tumor suppressor in liver cancer, leukemia and other tumors. In this, research, the promotion effect of the new compound synthesized in this research on the anti-cancer activity of LL-37 was evaluated.

As a kind of reactive and flammable highly gas, the acetylene (C₂H₂) is extensively utilized in cutting, welding, and lighting the metals (acetylene-oxygen flame).⁴ In these applications, high purity the C₂H₂ with high-purity is usually required; however, the impurities, for instance, methane (CH₄) and carbon dioxide (CO₂) always present in the production of acetylene.⁵ The critical temperature, sublimation point along with molecular size of CH₄, CO₂ and C₂H₂ are similar, which

[†]To whom correspondence should be addressed.
yangshuanyuan19692@163.com, ORCID[®]0000-0002-7783-261X
©2021 The Polymer Society of Korea. All rights reserved.

makes their separation challenging. As a result, the appearance of microporous materials containing the performances of selective adsorption (such as metal organic frameworks, MOFs) is a feasible choice in this field. MOFs as a novel type of porous materials, they are constructed from organic ligands and metal ions and reveal great potential in the catalysis, chemical separation, gas storage, molecular recognition, biomedicine, ion exchange, sensing and other fields.⁶⁻¹¹ With the assembly of given organic ligands and well-defined secondary building units, a variety of MOF architectures with low skeleton density, large specific surface area along with regular pore has been designed. In the past several years, the researchers are committed to fine-tuning the surrounding environments and pore architecture to investigate the practical application of MOFs.¹²⁻¹⁷ On the other hand, Zinc is an important biometal essential for life, which is second only to iron in terms of its concentration in the biological systems and is present in more than 300 enzymes of living organisms. Recent studies provided compelling evidence that Zn(II) derivatives have proved to be potential anticancer agents with low *in vivo* toxicity, low side effects and perhaps new modes of action and cellular targets compared with the classical metallodrugs. For instance, Azizollah and co-workers have studied the anticancer activity of two Zn(II)-based coordination complexes which scan be nominated as good anticancer agents against Caco-2 cell lines¹⁸; Mukherjee *et al.* have studied the anticancer activity or five mixed-ligand coordination polymers, and one of them demonstrates significant cell death toward human colorectal carcinoma cells.¹⁹ In the research, 5,5'-((5-carboxy-1,3-phenylene)bis(azanediyl))diisophthalic acid (H₅L) with the -NH-joints, a semi-rigid carboxylic acid ligand was chose for its Lewis basic N donor positions and rich π -electron-rich aryl parts, which offers latent binding positions to capture the C₂H₂. A fresh porous MOF based on Zn(II) has been triumphantly acquired, and its chemical formula is $\{[Zn_3(\mu_3\text{-OH})(L)(H_2O)_3] \cdot 3DEF \cdot H_2O\}_n$ (**1**), it was structurally investigated through powder X-ray diffraction (PXRD), the research of single crystal X-ray diffraction, infrared (IR) spectra, thermogravimetric analyses (TGA), as well as elemental analysis (EA). Owing to its Lewis basic -NH- joints and the π -electron-rich benzene rings on the skeleton, the activated complex **1** offers a favourable pore environment for binding C₂H₂ in preference to CO₂ and CH₄. At the environmental conditions, the adsorption capacity of C₂H₂ is up to 92.2 cm³ (STP) g⁻¹, while the ideal adsorbed solution theory (IAST)-predicted adsorption selectivity for the equivalent molar of C₂H₂-CO₂ and C₂H₂-CH₄

binary mixtures is as high as 4.5 and 30.6, respectively. The serial biological investigations were implemented to assess the compound's biological activity against liver cancer therapy combined with the LL-37. The molecular docking simulation is performed in addition to the experimental results for better understanding the origin of the possible anti-cancer activities of the proposed Zn complex.

Experimental

Chemicals and Measurements. All the reagents and solvents employed for the generation of the complex could be obtained from the market, and these could be exploited without processing. The FTIR spectra could be performed utilizing KBr pellets (5 mg sample in the KBr of 500 mg) with the infrared spectra region from 400 to 4000 cm⁻¹. Through employing Perkin-Elmer 240C analyzer (USA), we analyzed the Hydrogen, Nitrogen and Carbon elements. For the data of the PXRD, it could be recorded with Cu K α radiation via employing the X-ray diffractometer of Bruker D8 ADVANCE (with λ of 1.5418 Å, Germany), where X-ray tube was utilized at 40 mA and 40 kV. The TGA was implemented in the atmosphere of nitrogen at 5 °C·min⁻¹ heating rate exploiting the equipment of Seiko Extar 6000TG/DTA (Japan). For the as-generated samples, they can be characterized via utilizing TGA in the atmosphere of nitrogen at 10 K min⁻¹ heating rate exploiting the Perkin-Elmer Pyris 1 TGA thermogravimetric analyzer (USA) reached 873 K. Finally, the gas adsorption of C₂H₂, N₂, CH₄, and CO₂ were measured through the instrument of Micromeritics ASAP 2020 (American Micromeritics Corporation, USA).

Preparation and Characterization for $\{[Zn_3(\mu_3\text{-OH})(L)(H_2O)_3] \cdot 3DEF \cdot H_2O\}_n$ (1**).** 0.05 mmol and 24.1 mg of H₅L and 29.7 mg and 0.1 mmol of Zn(NO₃)₂·6H₂O were dissolved into the solvent mixture generated from 1 mL H₂O (1 mL) and diethylformamide (4 mL, DEF) (with 1:2 volum ratio). The product was autoclaved for seventy-two hours at 100 °C, and after that, it was naturally cooled to the environmental temperature in order to acquire the rectangular massive colorless crystals with 51 percent yield (on the basis of the Zn(ii)). Elemental analysis (%), calcd for the C₃₈H₅₃N₅O₁₈Zn₃: N, 6.58; C, 42.90 and H, 5.02. Found: N, 6.42%; C, 42.63% and H, 5.11%. IR (KBr, cm⁻¹): 586.1 (w), 627.9 (s), 655.8 (m), 695.2 (s), 743 (s), 779.9 (s), 809.3 (m), 851.2 (m), 872.1 (m), 969.8 (m), 1015.1 (s), 1060.5 (s), 1098.8 (s), 1123.3 (m), 1158.1 (s), 1193 (s), 1301.2 (s), 1364 (s), 1395.3 (m), 1426.7 (s), 1486 (s),

Table 1. The Details of Optimization and Its Parameters of Crystallography for Complex 1

Empirical formula	C ₂₃ H ₁₈ N ₂ O ₁₄ Zn ₃
Formula weight	742.50
Temperature (K)	293.0
Crystal system	Orthorhombic
Space group	<i>Pmm</i> 2 ₁
a (Å)	17.5714(2)
b (Å)	12.06380(10)
c (Å)	13.9417(2)
α (°)	90
β (°)	90
γ (°)	90
Volume (Å ³)	2955.33(6)
Z	2
ρ _{calc} (g/cm ³)	0.834
μ (mm ⁻¹)	1.242
Data/Restraints/Parameters	6885/13/199
Goodness-of-fit on <i>F</i> ²	1.020
Final <i>R</i> indexes, <i>I</i> >= 2σ(<i>I</i>)	<i>R</i> ₁ =0.0398, ω <i>R</i> ₂ =0.0951
Final <i>R</i> indexes, all data	<i>R</i> =0.0545, ω <i>R</i> ₂ =0.1013
Largest diff. peak/Hole (eÅ ⁻³)	0.43/-0.27
Flack parameter	0.000(7)
CCDC	2081423

1566.3 (s), 1625.6 (s), 1653.5 (s), 2930.2 (w), 3436 (br).

The data for X-ray can be analyzed through Oxford Xcalibur E diffractometer. For the strength data, it was analyzed via exploiting the CrysAlisPro, and this data was then converted to HKL files. And the original structural manners were established by the direct means based SHELXS, and after that, least-squares method based SHELXL-2014 was exploited to modify. The anisotropic parameters were mixed with global non-hydrogen atoms. Next, the entire hydrogen atoms were geometrically fixed via applying the AFIX commands to carbon atoms that they adjacent to. The compound's details of optimization and its parameters of crystallography were revealed in length in the Table 1.

Cell Counting Kit-8 kit (CCK-8). The CCK-8 detection kit was completed in the experiment for the assessment of the complex's inhibitory activity against the viability of the HepG2 liver cancer cells. This research was accomplished fully in the light of instructions with a little modification. Briefly, in the stage of logical growth phase, the HepG2 liver cancer cells could be harvested and then these cells were inoculated into

the plates of 96 well at 10⁵ cells each well ultimate destiny. After incubation for twelve hours in the incubator at 5% CO₂ and 37 °C, the treatment was completed after adding the compound into wells with 1-80 mM concentration. Subsequently, discarding the culture medium of cell and adding the fresh medium involving the reagent of CCK-8. At last, for each well, its absorbance was determined via using the microplate reader at 450 nm.

Trans-well Assay. For the sake of assessing the compound's influence against the invasion ability and the migration ability of HepG2 liver cancer cells, the trans-well assay was carried out in our work. This implementation was conducted total based on the protocols with minor change. In short, in the case of Matrigel matrix and no Matrigel matrix, the 24-well trans-well chambers was pre-coated. Then, the chambers were placed into the 24-well plates. Next, in the stage of logical growth phase, the HepG2 liver cancer cells could be harvested and then these cells were cultured into upper chamber in the medium without FBS at 5×10⁴ cells each well destiny. After the incubation of cells in the incubator at 5 percent CO₂ and 37 °C temperature, after twenty-four hours, the remaining cells in upper parts of membranes were wiped off carefully, and the cells in lower part of membranes were labeled with crystal violet (0.5%). Under the microscope and in 6 randomly separated fields, the numbers of cells on the lower membrane surface was quantified. This conduction was carried out at least 3 times.

Simulation Details. The grid parameter file for the molecular docking simulation that contains the binding area and the Zn complex is prepared by AutoDockTools ver. 1.5.6., the binding area that contains multiple residues where the active binding sites are determined is from the protein 1WQ8 (PDB code), which is a member of the vascular endothelial growth factor-A (VEGF) protein family. The binding area coordinates are 19.606, 31.676, and 0.317 in three dimensions and the length of the cubic box is 80 angstrom. The docking parameter file for the molecular docking simulation has also been prepared by AutoDockTools, the Zn complex has 3 rotatable dihedrals and the maximum allowed binding poses are set to 50 for better sampling. All simulations are performed by AutoDock ver. 4.2. The post-analysis and visualization are performed by PyMOL ver. 2.2.

Results and Discussion

Structural Characterization. The complex 1 could be gen-

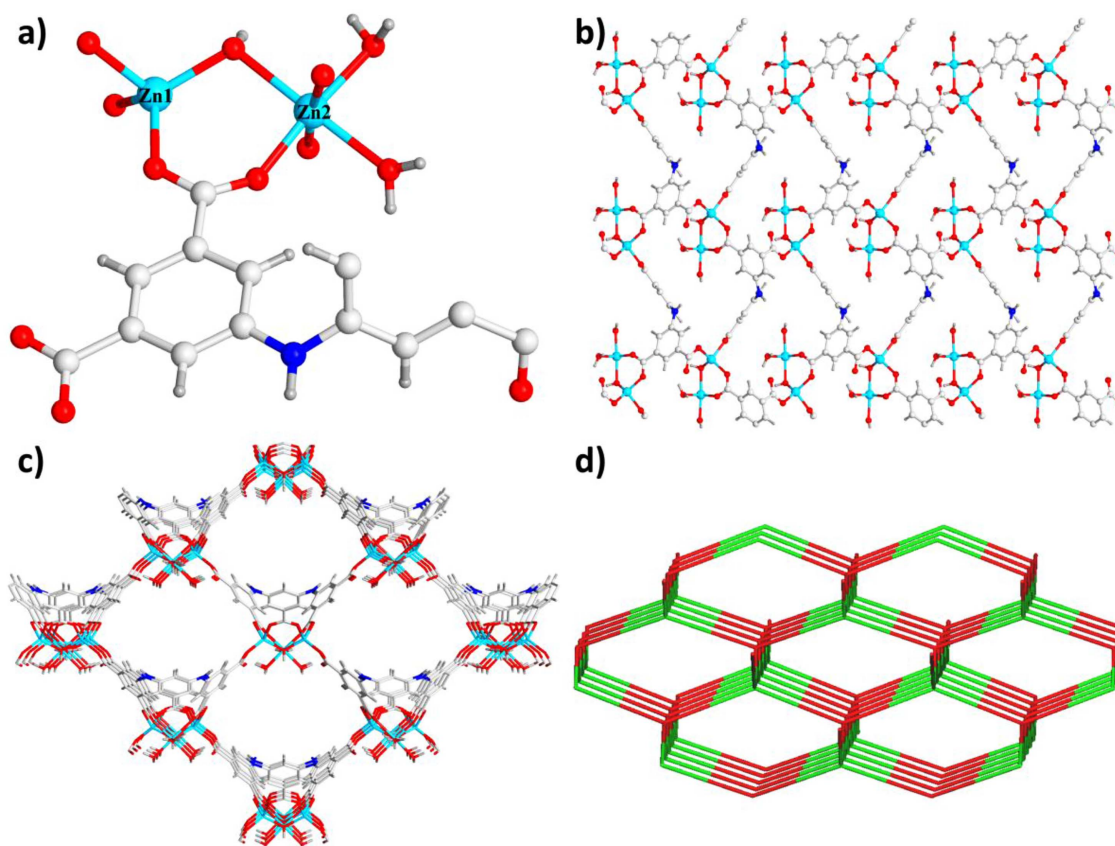


Figure 1. (a) The compound **1**'s asymmetry unit; (b) The two-dimensional layered net of complex **1**; (c) The **1**'s three-dimensional net reflecting the one-dimensional channels; (d) The four-linked topological net of complex **1**.

erated with the solvothermal reaction between $\text{Zn}(\text{NO}_3)_2 \cdot 6\text{H}_2\text{O}$ and H_3L in the water and DEF mixed solvent for 72 h at 100 °C, which was created as the light yellow crystals, and its chemical formula is $\{[\text{Zn}_3(\mu_3\text{-OH})(\text{L})(\text{H}_2\text{O})_3] \cdot 3\text{DEF} \cdot \text{H}_2\text{O}\}_n$ (**1**) on the basis of the outcomes from the research of single crystal X-ray diffraction, EA and TGA. Based on the data of single crystal acquired at the environmental temperature, the outcomes of optimization and the solution of structure indicate that in $Pmn2_1$ space group of orthorhombic system, the **1** could crystallize. And each of the asymmetric unit includes 1.5 separated Zn(ii) atoms in crystallography, 0.5 ligand of L^{5-} , $\text{ab}\mu_3\text{-OH}$, along with 0.5 molecules of H_2O (Figure 1(a)). The Zn1 atom was coordinated through 3 carboxylic O atoms in 3 diverse ligands of L^{5-} and a $\mu_3\text{-OH}$ O atom. The architecture reflected a slightly distorted coordination geometry and tetrahedron. While the Zn2 atom created a twisted or distorted geometry of octahedron with 2 O atoms originated from 2 distinct ligands of L^{5-} , a $\mu_3\text{-OH}$ O atom as well as 3 O atoms derived from 3 diverse lattice molecules of water. Furthermore, the Zn1#3, Zn2 and Zn1 atoms shared $\mu_3\text{-OH}$ O atom in order

to generated the trinuclear nodes of $[\text{Zn}_3(\mu_3\text{-OH})(\text{H}_2\text{O})_3(\text{COO})_5]$, in which, the bond length of Zn-O is between 1.91 Å and 2.18 Å. The completely deprotonated L^{5-} ligand carboxylic acid groups connected Zn1 with the $\mu_1\text{-}\eta^1:\eta^1$ and $\mu_2\text{-}\eta^1:\eta^1$ bridging manners to create one-dimensional infinite chains. Afterwards, the one-dimensional chains connected to each other to generated a two-dimensional layer (Figure 1(b)), which furthermore was in-depth fused via Zn2, Zn1, and the ligands of H_3L into a three-dimensional architecture. As the calculation with the program of PLATON, the complex **1**'s solvent-accessible void volume was 69.5 percent without considering the coordinated and lattice solvents. This 3D skeleton composed of $7.99 \text{ \AA} \times 10.13 \text{ \AA}$ honeycomb cavities, and the Lewis -NH-moieties and π -electron-rich benzene rings of ligands were uniformly distributed in the pore inner walls. These might utilize as interaction positions for the bindings of C_2H_2 (Figure 1(c)). For the sake of acquiring a better understanding of skeleton, both the ligands of L^{5-} and trinuclear nodes were classified as the four-linked nodes, thus the complex **1** could be viewed as the uninodal network with (6^6) topological point symbol (Fig-

ure 1(d)).

At the aim of checking the products' phase purity, the research of PXRD on the compound produced was implemented (Figure 2(a)). For simulated PXRD manners, its peak positions are in accordance with the experiment results, and this reflects that the crystal structure is the genuine representative of the whole product of the crystal. For the crystal samples, its selective selection will result in the difference in the strength of product. For the complex **1** generated, the TGA was implemented to assess its thermodynamic stability between 25 and 800 °C under the atmosphere of nitrogen. As displayed in the Figure 2(b), the complex **1**'s TGA curve reveals a continuous weightlessness of 34.8 percent (the calculated value is 35.3 percent) between 30 °C and 270 °C, which equivalent to the release of captured guest solvent molecules (3 DEF and a H₂O) and the coordinated molecules of H₂O, then there is a relatively stable platform. After reaching 370 °C, the frame begins to form. The porosity parameters were characterized by N₂ desorption and adsorption experiments at 77 K. At the aiming of removing solvent molecules in pores, the prepared **1** was exchanged by the dry low-boiling acetone and then desolved at 373 K in high vacuum until reached 3 μmHg·min⁻¹ degassing

rate. The analysis of PXRD showed that activation treatment had no influence on the structural integrity and crystallinity. As revealed in the Figure 2(c), **1a** reflected that in the region of low relative pressure, the amount of N₂ absorption increased sharply, followed by the platform, and the total amount of N₂ absorption per gram was 301 cm³ (STP). In accordance with the classification of IUPAC, the adsorption isotherm is classical type-I, which exhibits that the micropore structure is good. According to the adsorption data, the specific surface areas of Langmuir and BET (Brunauer-Emmett-Teller) were 1303 m²·g⁻¹ and 1180 m²·g⁻¹, respectively. The distribution analysis of pore size according to the DFT pattern exhibited 3 main peaks centered at 7.3 Å (Figure 2(d)), which is equivalent to the cage sizes described in previous analysis of structure.

Selective Gas Sorption Properties. Considering the construction of the intrinsic permanent porosity and the distribution of Lewis -NH- parts and π-electron-rich benzene rings of ligand as the recognition sites of C₂H₂ in inner wall, we investigated the latent application of the **1a** as adsorbent for the CH₄ and CO₂ separation from the C₂H₂. As a result, the isotherms of single-component adsorption-desorption isotherms of CO₂, C₂H₂, and CH₄ were harvested at 3 distinct temperatures

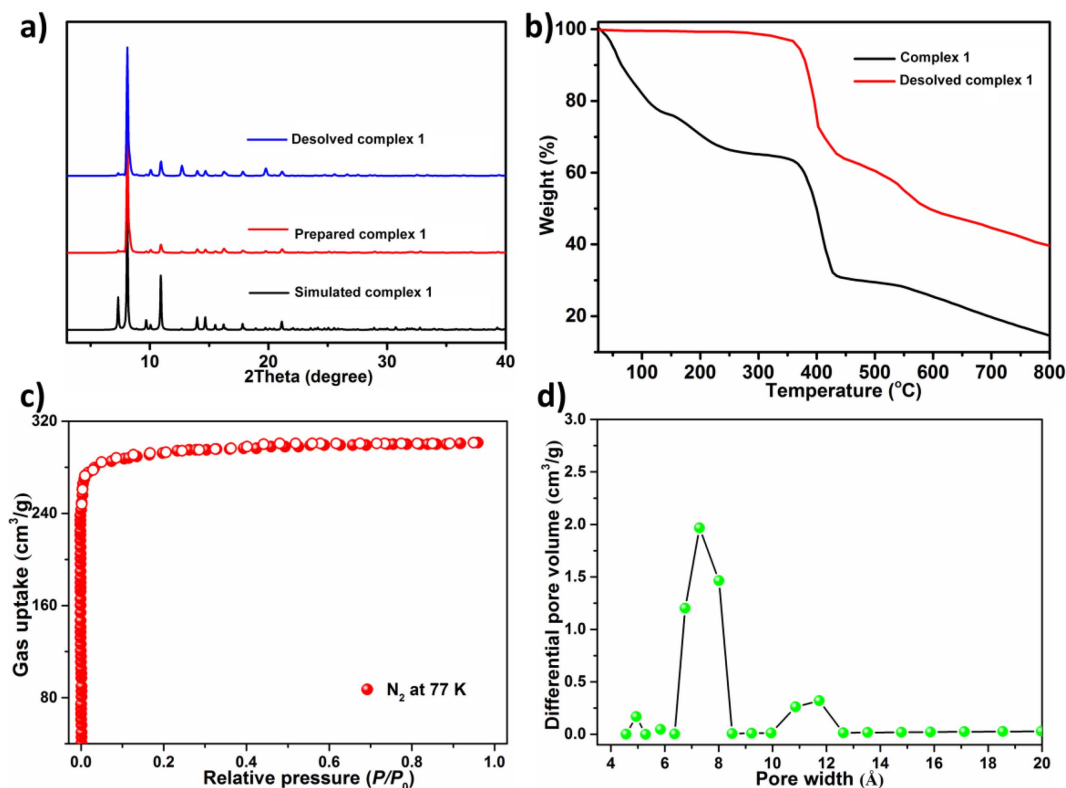


Figure 2. (a) The complex **1**'s PXRD manners; (b) The diagram of TGA curve for the complex **1**; (c) The N₂ adsorption curve at 77 K of the **1a**; (d) The distribution of pore size calculated via the DFT approach.

of 298 K and 273 K along with pressure of 1 atm (Figure 3(a) and Figure 3(d)). At 1 atm pressure, the absorption capacities of CH₄, CO₂, and C₂H₂ of **1** were 30.1, 83.2, and 92.3 cm³ (STP) g⁻¹ at 298 K, respectively, and at 273 K, increased to 43.4, 106.3, and 102.5 cm³ (STP) g⁻¹ owing to the process of exothermic physical adsorption. It was found that the C₂H₂ absorption for the **1a** at 1 atm and 298 K exceeded that of most reported porous MOFs with no open metal positions, for instance, ZIF-8, MOF-5, BSF-1, [Zn₁₂(tdc)₆(glycerol)₆(dabco)₃], and UTSA-36, and their absorption respectively are 25, 26, 52.6, 55.1, and 56.8 cm³ (STP) g⁻¹. We are glad that **1a** can adsorb much more C₂H₂ than CH₄ and CO₂, particularly at low pressure. For instance, at 0.5 bar, the actual gas mixture encounters classical C₂H₂ partial pressure, and at 273 K, the molar ratios of adsorbed C₂H₂/CO₂ and C₂H₂/CH₄ are 1.2 and 3.6, and enhanced to 1.5 and 5.2 at 298 K, respectively.

In addition to the difference of adsorption capacity, the affinity of **1a** for CH₄, CO₂ and CH₄ also has obvious difference in the slope of isotherm in the region of low pressure region. For the C₂H₂ isotherm, its slope is much larger than that of CH₄ and CO₂ isotherm, suggesting that the interaction between the

skeleton and C₂H₂ is stronger than that of CH₄ and CO₂. In order to quantify the affinity between adsorbate and adsorbent, the loading-dependent isotherm (Q_{st}) of CH₄, CO₂ and C₂H₂ adsorption could be extracted from the isotherm of temperature-dependent gas in accordance with the virus equation, as shown in Figure 3(c), as a gas loadings function. In the whole process of adsorption, the Q_{st} value of C₂H₂ was significantly higher than the value of CH₄ and CO₂. Specifically, at approximately 0 surface loadings, the values of Q_{st} for CH₄, CO₂ and CH₄ are 22.2±2.2, 26.2±0.1, and 32.4±0.2 kJmol⁻¹, respectively.

As explored above, the intensity and adsorption capacity of **1a** were CH₄ < CO₂ < CH₄, suggesting that the **1a** could be utilized as the adsorbent for the separations of C₂H₂/CH₄ and C₂H₂/CO₂. In order to explain this point, we apply the famous IAST pattern proposed via Prausnitz and Myers to predict adsorption selectivity from determined single-component isotherms in experiment, because the adsorption selectivity is a significant criterion for assessing the gas separation property of the specified adsorbent. The data of isotherm can be associated with the single-point equation of Langmuir-Freundlich. The

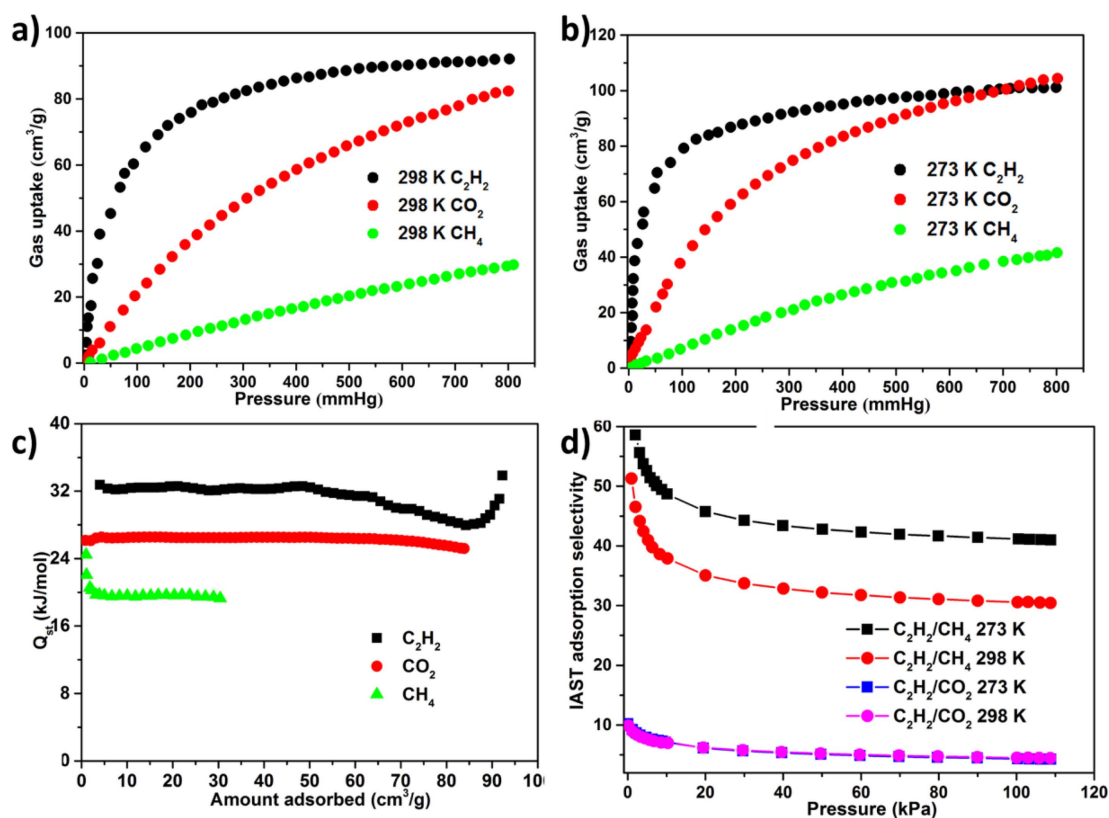


Figure 3. The adsorption profiles for CH₄, CO₂ and C₂H₂ at (a) 298 K; (b) 273 K; (c) The isothermic heat of CH₄, CO₂, and C₂H₂ adsorbed in the **1a** is related to the gas loading; (d) The IAST selectivity for C₂H₂/CO₂ and C₂H₂/CH₄ at 298 and 273 K.

acquiring fitting parameters are employed for the calculation of the IAST selectivity. Figure 3(d) reflected the adsorption selectivity of C_2H_2/CH_4 and C_2H_2/CO_2 equivalent molar binary mixtures at two diverse temperatures. It can be found that adsorption selectivity is decided by the temperature along with total gas pressure. The adsorption selectivities of C_2H_2/CH_4 and C_2H_2/CO_2 reduced with the enhancement of total pressures. The reasons can be reflected as follows. At low pressure, the C_2H_2 molecule is easy to take over the primary adsorption positions. With the enhancing pressure, the adsorption positions of C_2H_2 are less and less. Therefore, the selectivity reduces accordingly. With the reduction of temperature, the adsorption selectivity of C_2H_2/CH_4 increased, while the adsorption selectivity of C_2H_2/CO_2 maintained nearly unchanged. With an atmospheric pressure, the adsorption selectivity of C_2H_2/CO_2 and C_2H_2/CH_4 is up to 4.3 and 41.2 at 278 K, 4.5 and 30.6 at 298 K, respectively. Despite the adsorption selectivities of C_2H_2/CO_2 and C_2H_2/CH_4 are not the highest values reported so far, these values are even higher than or still comparable to the values of some MOFs, for instance, $[Zn_{12}(tdc)_6(\text{ethylene glycol})_6(\text{dabco})_3]$ ($C_2H_2/CO_2=3.3$), UTSA-68 ($C_2H_2/CO_2=3.4$), BSF-1 ($C_2H_2/CO_2=3.3$), and ZJNU-100 ($C_2H_2/CO_2=3.81$). In conclusion, the high adsorption selectivity of C_2H_2 for CH_4 and CO_2 and the high adsorption of C_2H_2 give **1a** a potential application prospect as the solid adsorbent for the CH_4 and CO_2 separation from C_2H_2 under environmental conditions.

Compound Significantly Reduced the Viability of the Liver Cancer Cells. After creating the new compound, its anti-cancer activity combined with the LL-37 was firstly eval-

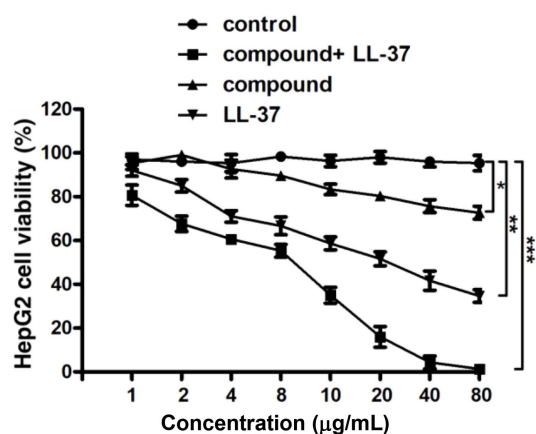


Figure 4. Remarkably declined liver cancer cells viability after the treatment of compound. The CCK-8 was applied for the assessment of the liver cancer cells viability.

uated. Cancer cells are characterized by abnormal proliferation, therefore, in our investigation, the liver cancer cells viability after the treatment via the compound combined with LL-37 was detected through the CCK-8 assay. The outcomes reflect in the Figure 4 revealed that the compound combined with LL-37 could distinctly decline the cancer cells viability, in comparison with control group.

Compound Obviously Inhibited the Migration and Invasion Ability of the Liver Cancer Cells. In the previous study, the compound with LL-37 showed excellent inhibitory activity on the liver cancer cells viability. Furthermore, the compound plus LL-37 influence against the invasion ability and migration ability of cancer cell still required to be inves-

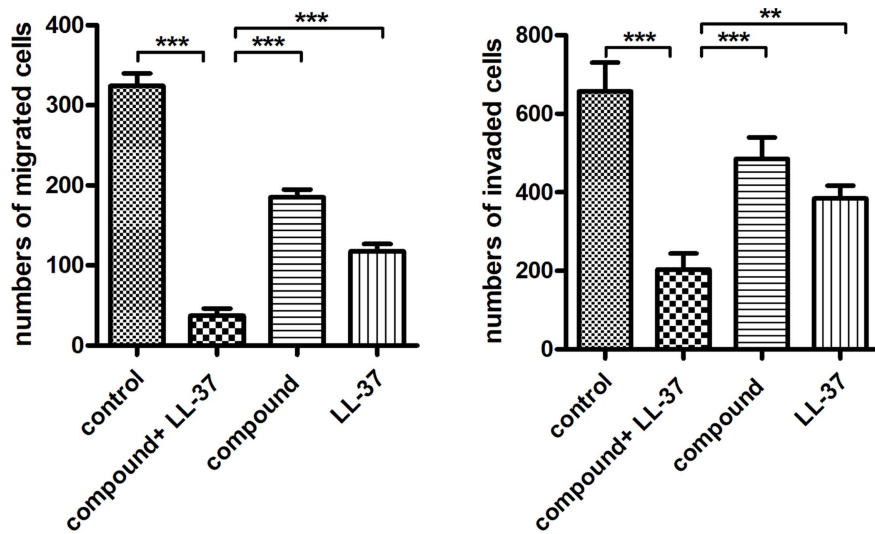


Figure 5. Obviously inhibited invasion ability and migration ability for the liver cancer cells after treating through the compound. The transwell assay was conducted to assess the compound effect on the invasion ability and migration ability of cancer cell.

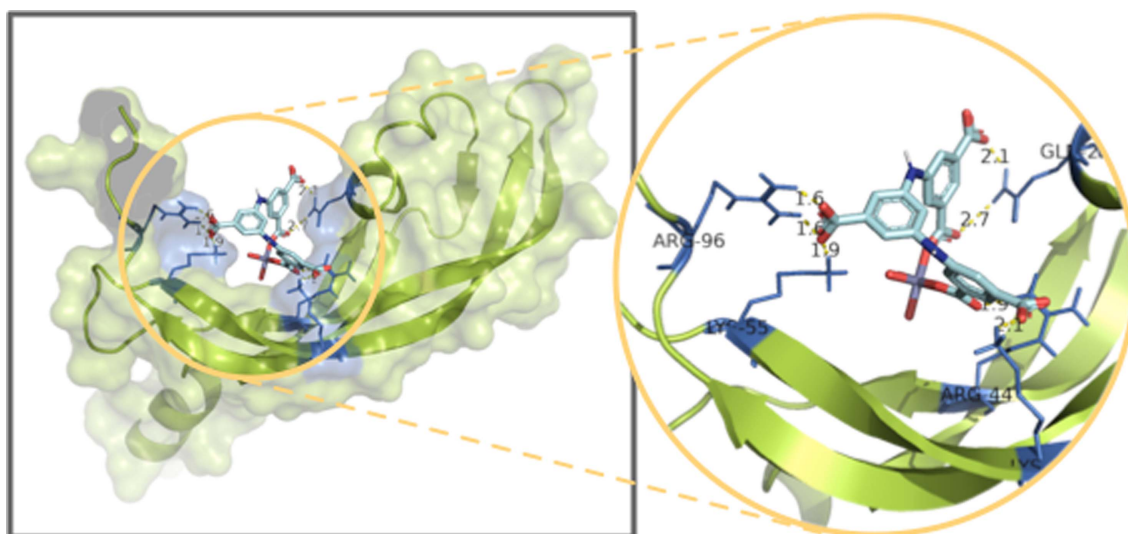


Figure 6. The favorable conformation between the coordination polymer and the protein.

tigated. Hence, the trans-well assay was carried out in our experiment. As the data reflected in the Figure 5, we can observe the liver cancer cells has a relatively stronger invasion ability and migration ability, in contrast to normal liver cells. After compound and LL-37 treatment, the invasion ability and migration ability for the liver cancer cells was obviously declined.

Molecular Docking. The vascular endothelial growth factor has multiple effects when binding to kinase insert domain-containing receptor,²⁰ which has been used as probe protein for identifying the activities of the proposed drug molecule upon the anti-cancer treatment. Thus, in the current study, the crystal structure 1WQ8 of VEGF has been used as the target protein for the molecular docking simulation. There are 50 possible allowed binding poses for estimating the binding interactions, and the one which is the energetically favorable binding conformation is analyzed in detail and is shown in Figure 6.

As shown in Figure 6, the most advantageous binding conformation is shown and the estimated binding affinity energy is -8.51 kcal/mol. It can be obviously seen from the surface view that there are multiple binding interactions generated between the target protein 1WQ8 and Zn complex. In the magnified local binding view, it is observed that there are 7 binding interactions formed in total, and the binding distances are varying from 1.6 to 2.7 angstrom, indicating a strong binding strength is obtained. Explicitly, the carbonyl oxygens from the Zn complex are the donors of the hydrogen bonds, and the receptors are residues ARG-96, LYS-55, ARG-44, LYS-61 and GLN-25. Such results suggest that the proposed Zn complex

has excellent stabilization effect on the given probe protein and therefore exhibits good anti-cancer activities.

Conclusions

To sum up, we have created a fresh porous Zn-MOF with employment of 5,5'-((5-carboxy-1,3-phenylene)bis(azanediyl))-diisophthalic acid (H₅L) with the -NH- joints, a semi-rigid carboxylic acid ligand. Owing to its Lewis basic -NH- joints and the π -electron-rich benzene rings on the skeleton, the activated complex **1** offers a favourable pore environment for binding C₂H₂ in preference to CO₂ and CH₄. At the environmental conditions, the adsorption capacity of C₂H₂ is up to 92.2 cm³ (STP) g⁻¹, while the IAST-predicted adsorption selectivity for the equivalent molar of C₂H₂-CO₂ and C₂H₂-CH₄ binary mixtures is as high as 4.5 and 30.6, respectively. The CCK-8 kit outcomes indicated that this compound could distinctly decline the liver cancer cells viability. Furthermore, the invasion ability and migration ability for the liver cancer cells was also decreased under the cancer cell exposure. Finally, it can be acquired that this compound was an outstanding candidate for the liver cancer treatment through inhibiting the viability, invasion ability and migration ability of the cancer cells. The performed molecular docking simulation showed that multiple hydrogen bonds were formed between the proposed Zn complex and the VEGF protein, the binding lengths are between 1.6 and 2.7 angstrom. Such results indicate that the Zn complex has good anti-cancer activities and shows good potential for cancer treatment.

References

- Gravitz, L. Liver Cancer. *Nature* **2014**, 516, S1.
- Marengo, A.; Rosso, C.; Bugianesi, E. Liver Cancer: Connections with Obesity, Fatty Liver, and Cirrhosis. *Annu. Rev. Med.* **2016**, 67, 103-117.
- Anwanwan, D.; Singh, S. K.; Singh, S.; Saikam, V.; Singh, R. Challenges in Liver Cancer and Possible Treatment Apches. *Biochim. Biophys. Acta Rev. Cancer* **2020**, 1873, 188314.
- Zeng, H.; Xie, M.; Huang, Y.; Zhao, Y.; Xie, X.; Bai, J.; Wan, M.; Krishna, R.; Lu, W.; Li, D. Induced Fit of C₂H₂ in a Flexible MOF Through Cooperative Action of Open Metal Sites. *Angew. Chemie Int. Ed.* **2019**, 58, 8515-8519.
- Li, Y. T.; Zhang, J. W.; Lv, H. J.; Hu, M. C.; Li, S. N.; Jiang, Y. C.; Zhai, Q. G. Tailoring the Pore Environment of a Robust Ga-MOF by Deformed [Ga₃O(COO)₆] Cluster for Boosting C₂H₂ Uptake and Separation. *Inorg. Chem.* **2020**, 59, 10368-10373.
- Fan, W.; Wang, X.; Liu, X.; Xu, B.; Zhang, X.; Wang, W.; Wang, X.; Wang, Y.; Dai, F.; Yuan, D.; Sun, D. Regulating C₂H₂ and CO₂ Storage and Separation through Pore Environment Modification in a Microporous Ni-MOF. *ACS Sustain. Chem. Eng.* **2019**, 7, 2134-2140.
- Feng, X.; Li, R. F.; Wang, L. Y.; Ng, S. W.; Qin, G. Z.; Ma, L. F. A Series of Homonuclear Lanthanide Coordination Polymers Based on a Fluorescent Conjugated Ligand: Syntheses, Luminescence and Sensor. *CrystEngComm* **2015**, 17, 7878-7887.
- Feng, X.; Feng, Y. Q.; Liu, L.; Wang, L. Y.; Song, H. L.; Ng, S. W. A Series of Zn-4f Heterometallic Coordination Polymers and a Zinc Complex Containing a Flexible Mixed Donor Dicarboxylate Ligand. *Dalton Trans.* **2013**, 42, 7741-7754.
- Fan, L.; Zhao, D.; Li, B.; Chen, X.; Wang, F.; Deng, Y.; Niu, Y.; Zhang, X. An Exceptionally Stable Luminescent Cadmium(II) Metal-Organic Framework as Dual-functional Chemoensor for Detecting Cr(VI) Anions and Nitro-containing Antibiotics in Aqueous Media. *CrystEngComm* **2021**, 23, 1218-1225.
- Hu, M. L.; Abbasi-Azad, M.; Habibi, B.; Rouhani, F.; Moghanni-Bavil-Olyaei, H.; Liu, K. G.; Morsali, A. Electrochemical Applications of Ferrocene-Based Coordination Polymer, *ChemPlusChem* **2020**, 85, 2397-2418.
- Hu, M. L.; Razavi, S. A.; Piroozzadeh, M.; Morsali, A. Sensing Organic Analytes by Metal-organic Frameworks: A New Way of Considering the Topic. *Inorg. Chem. Front.* **2020**, 7, 1598-1632.
- Hu, M. L.; Mohammad, Y. M.; Morsali, A. Template Strategies with MOFs. *Coord. Chem. Rev.* **2019**, 387, 415-435.
- Zhang, J.; Zhao, J.; Sun, Y.; Xin, M.; Zhang, D.; Bian, R. Mechanisms of Emerging Pollutant Dechlorane Plus on the Production of Short-chain Fatty Acids from Sludge Anaerobic Fermentation. *Environ. Sci. Pollut. R.* **2021**, 28, 34902-34912.
- Xu, H.; Du, H.; Kang, L.; Cheng, Q.; Feng, D.; Xia, S. Constructing Straight Pores and Improving Mechanical Properties of GangeBased Porous Ceramics. *J. Renew. Mater.* **2021**, 9, 2129-2141.
- Duan, C.; Yu, Y.; Li, J.; Li, L.; Huang, B.; Chen, D.; Xi, H. Recent Advances in the Synthesis of Monolithic Metal-organic Frameworks. *Sci. China Mater.* **2021**, 64, 1305-1319.
- Wang, D.; Liu, B.; Yao, S.; Wang, T.; Li, G.; Huo, Q.; Liu, Y. A Polyhedral Metal-organic Framework Based on the Supermolecular Building Block Strategy Exhibiting High Performance for Carbon Dioxide Capture and Separation of Light Hydrocarbons. *Chem. Commun.* **2015**, 51, 15287-15289.
- Lee, J. H.; Lee, H. J.; Lim, S. Y.; Kim, B. G.; Choi, J. W. Combined CO₂-philicity and Ordered Mesoporosity for Highly Selective CO₂ Capture at High Temperatures. *J. Am. Chem. Soc.* **2015**, 137, 7210-7216.
- Beheshti, A.; Bahrani-Pour, M.; Kolahi, M.; Shakerzadeh, E.; Motamedi, H.; Mayer, P. Synthesis, Structural Characterization, and Density Functional Theory Calculations of the Two New Zn(II) Complexes as Antibacterial and Anticancer Agents with a Neutral Flexible Tetradentate Pyrazole-based Ligand. *Appl. Organomet. Chem.* **2021**, 35, e6173.
- Mukherjee, S.; Ganguly, S.; Manna, K.; Mondal, S.; Mahapatra, S.; Das, D. Green Approach To Synthesize Crystalline Nanoscale Zn(II)-Coordination Polymers: Cell Growth Inhibition and Immunofluorescence Study. *Inorg. Chem.* **2018**, 57, 4050-4060.
- Suto, K.; Yamazaki, Y.; Morita, T.; Mizuno, H. Crystal Structures of Novel Vascular Endothelial Growth Factors (VEGF) from Snake Venoms. *J. Biol. Chem.* **2005**, 280, 2126-2131.

Publisher's Note The Polymer Society of Korea remains neutral with regard to jurisdictional claims in published articles and institutional affiliations.